frontiers | Frontiers in Chemistry

ORIGINAL RESEARCH
published: 14 April 2022
doi: 10.3389/fchem.2022.857863

Asymmetric Dissociative Tunneling Ionization of Tetrafluoromethane in $\omega - 2\omega$ Intense Laser Fields

*Hiroka Hasegawa[1], Tiffany Walmsley[1,2], Akitaka Matsuda[1], Toru Morishita[3], Lars Bojer Madsen[4], Frank Jensen[5], Oleg I. Tolstikhin[6] and Akiyoshi Hishikawa[1,7]**

[1]Graduate School of Science, Nagoya University, Nagoya, Japan, [2]School of Chemistry, University of Edinburgh, Edinburgh, United Kingdom, [3]Institute for Advanced Science, The University of Electro-Communications, Chofu-shi, Tokyo, Japan, [4]Department of Physics and Astronomy, Aarhus University, Aarhus, Denmark, [5]Department of Chemistry, Aarhus University, Aarhus, Denmark, [6]Moscow Institute of Physics and Technology, Dolgoprudny, Russia, [7]Research Center for Materials Science, Nagoya University, Nagoya, Japan

Dissociative ionization of tetrafluoromethane (CF_4) in linearly polarized ω-2ω ultrashort intense laser fields (1.4×10^{14} W/cm^2, 800 and 400 nm) has been investigated by three-dimensional momentum ion imaging. The spatial distribution of CF_3^+ produced by $CF_4 \rightarrow CF_3^+ + F + e^-$ exhibited a clear asymmetry with respect to the laser polarization direction. The degree of the asymmetry varies by the relative phase of the ω and 2ω laser fields, showing that 1) the breaking of the four equivalent C-F bonds can be manipulated by the laser pulse shape and 2) the C-F bond directed along the larger amplitude side of the ω-2ω electric fields tends to be broken. Weak-field asymptotic theory (WFAT) shows that the tunneling ionization from the $4t_2$ second highest-occupied molecular orbital (HOMO-1) surpasses that from the $1t_1$ HOMO. This predicts the enhancement of the tunneling ionization with electric fields pointing from F to C, in the direction opposite to that observed for the asymmetric fragment ejection. Possible mechanisms involved in the asymmetric dissociative ionization, such as post-ionization interactions, are discussed.

Keywords: coherent control, intense laser fields, tunneling ionization, molecular dissociation, tetrafluoromethane

OPEN ACCESS

Edited by:
Yuichi Fujimura, Tohoku University, Japan

Reviewed by:
Hideki Ohmura, National Institute of Advanced Industrial Science and Technology (AIST), Japan
Hirohiko Kono, Tohoku University, Japan

****Correspondence:***
Akiyoshi Hishikawa
hishi@chem.nagoya-u.ac.jp

Specialty section:
This article was submitted to Physical Chemistry and Chemical Physics, a section of the journal Frontiers in Chemistry

Received: *19 January 2022*
Accepted: *22 February 2022*
Published: *14 April 2022*

Citation:
Hasegawa H, Walmsley T, Matsuda A, Morishita T, Madsen LB, Jensen F, Tolstikhin OI and Hishikawa A (2022) Asymmetric Dissociative Tunneling Ionization of Tetrafluoromethane in $\omega - 2\omega$ Intense Laser Fields. Front. Chem. 10:857863. doi: 10.3389/fchem.2022.857863

1 INTRODUCTION

Shaped intense laser fields with a field intensity of $\sim 10^{14}$ W/cm^2 have attracted considerable attention in the last decades for their capability to manipulate ultrafast electronic and nuclear dynamics of atoms, molecules, and solids. Armed with the electric field exerting a force on the electrons comparable to that of the Coulomb potential in a molecule, shaped laser pulses enable us to drive electrons in a nonperturbative manner to exploit unique properties from the targets. The application has been demonstrated in controls of high-order harmonic generation (Bartels et al., 2000; Pfeifer et al., 2005; Winterfeldt et al., 2008), photoemission (Bardeen et al., 1997; Wollenhaupt and Baumert, 2011; Eickhoff et al., 2021), and chemical reactions (Levis et al., 2001; Assion et al., 1998; Levis and Rabitz, 2002; Hishikawa et al., 2020).

Laser pulse shaping can be accomplished by a spatial amplitude and phase modulator placed on a Fourier transform plane in a 4*f* setup (Bardeen et al., 1997; Levis et al., 2001; Assion et al., 1998; Eickhoff et al., 2021). Alternatively, one can synthesize the laser waveform by coherent superposition of pulses with different colors (Chan et al., 2011; Manzoni et al., 2015), which has been used to control high harmonic generation (Takahashi et al., 2010; Neyra et al., 2018) and multiphoton and tunneling ionization of atoms and molecules (Eickhoff et al., 2021; Ohmura and Saito, 2020; Ohmura et al., 2021). Among others, the ω-2ω laser fields, consisting of the fundamental and the second harmonics, have been

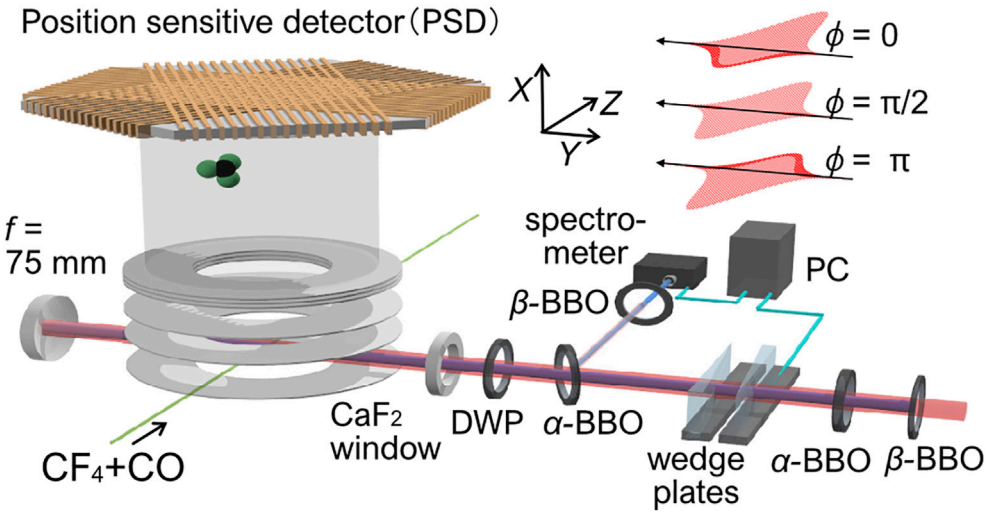

FIGURE 1 | Schematic of the experimental setup. The output from a Ti: Sapphire regenerative laser amplifier system (800 nm, 1 kHz, 50 fs) was introduced to a β-BBO crystal (type-I) to generate a second-harmonic pulse (400 nm). The time delay between the fundamental (ω) and the second harmonics (2ω) pulse was compensated by two birefringent α-BBO crystals. The two-color relative phase was stabilized by a pair of fused-silica wedge plates controlled by the active feedback locking to the 2ω-2ω interference spectrum. The polarization of the fundamental and the second harmonic pulse was set parallel by a dual-wavelength plate (DWP). For the phase calibration, CO gas is mixed with the sample gas of CF_4.

widely used for understanding the mechanisms of laser tunneling ionization and chemical reaction control in intense laser fields. In the case of linear polarization along the Z direction, the ω-2ω electric fields may be expressed as follows (Endo et al., 2019):

$$\mathbf{F}(t) = F(t)\mathbf{e}_Z, \tag{1}$$

$$F(t) = \bar{F}_\omega(t)\cos(\omega t) + \bar{F}_{2\omega}(t)\cos(2\omega t + \phi), \tag{2}$$

where $\bar{F}_\omega(t)$ and $\bar{F}_{2\omega}(t)$ represent the envelopes of the fundamental and the second harmonic pulses, respectively, and ϕ is the two-color relative phase. The unit vector along the Z-axis is denoted as $\mathbf{e}_Z$. Typical ω-2ω electric fields are illustrated in **Figure 1**, showing that the direction and degree of asymmetry vary by phase ϕ for a given ratio of the ω and 2ω field intensities.

Asymmetric fragment ejection through directional bond-breaking has been observed for various molecules in the ω-2ω intense laser fields. For HD (Sheehy et al., 1995), NO (Endo et al., 2019; Li et al., 2011), CO (Li et al., 2011; Ohmura et al., 2011; Ohmura et al., 2014), OCS (Ohmura et al., 2014; Endo et al., 2022), and CH_3X (X = F, Cl, Br, I) (Ohmura et al., 2006a; Ohmura et al., 2006b; Walt et al., 2015), the directional fragment ejection has been observed. The observed asymmetric distribution of fragment ions is interpreted as a result of orientation-selective tunneling ionization followed by dissociation in intense ω-2ω laser fields. Molecular tunneling ionization has been discussed intensively in the last decade, showing that many of the characteristic properties can be understood in terms of the shape of molecular orbitals (MOs) and their direction of electric dipole moments. Because of the asymmetric MOs and the non-zero dipole moments of the linear heteronuclear molecules mentioned above, tunneling ionization is enhanced in one direction along the molecular axis compared to the other, resulting in orientation-selective ionization.

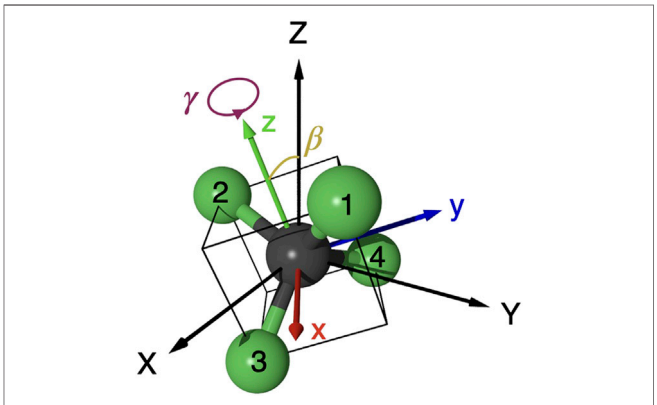

FIGURE 2 | Molecular orientation of CF_4 in the laboratory frame (X, Y, Z), where the polarization direction of the linearly polarized $\omega-2\omega$ laser fields is directed along the Z-axis. The molecular principal axis (C_2 axis) is along the z-axis of the molecular frame (x, y, z). The orientation is specified by the Euler angles (α, β, γ). Because of the axial symmetry around the electric field F one can set α=0 without losing generality.

The asymmetric fragment ejection is also observed with symmetric molecules such as D_2 (Ray et al., 2009; Wanie et al., 2015), H_2O (Kechaoglou et al., 2019), CO_2 (Endo et al., 2016; Endo et al., 2017), and C_2H_2 (Song et al., 2015). For D_2 (Ray et al., 2009; Wanie et al., 2015), electron localization is induced by the coherent superposition of two cationic states through interaction with two kinds of photons of the fundamental and second harmonic, resulting in asymmetric D^+ ejection. For C_2H_2 (Song et al., 2015), H^+ ejection associated with breaking the C-H bond shows clear asymmetry with respect to the laser polarization. The observed selectivity is suggested to be produced

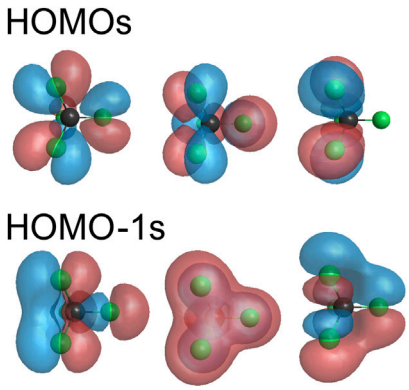

FIGURE 3 | Highest-occupied molecular orbitals HOMO ($1t_1$) and HOMO-1 ($4t_2$). Both HOMO and HOMO-1 are triply degenerated.

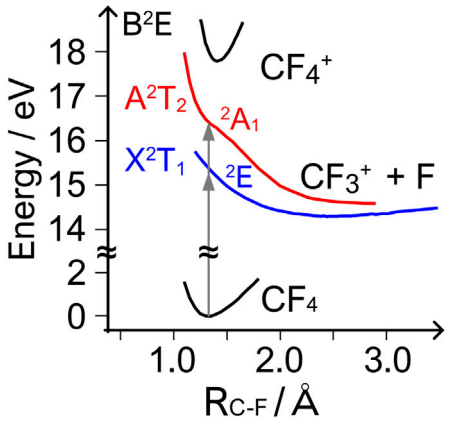

FIGURE 4 | Schematic potential energy curves of selected electronic states of CF_4 and CF_4^+ as a function of the internuclear distance $R_{C\text{-}F}$ between F and C in the CF_3 group [reproduced from Tang et al. (2013)].

by laser-induced coupling of HOMO and HOMO-1, 2 states. For CO_2 (Endo et al., 2016; Endo et al., 2017), asymmetric ejection of O^+ was observed on the larger amplitude side of the ω-2ω laser fields. This is consistent with the results of a theoretical calculation of nuclear wave packet dynamics on the potential energy surfaces (PES) of CO_2^{2+} in ω-2ω intense laser fields (Sato et al., 2003), demonstrating the chemical reaction control by laser manipulation of PES.

This study discusses the feasibility of applying the ω-2ω reaction control to more complex symmetric molecules. More specifically, we study a tetrahedral molecule, tetrafluoromethane (CF_4), which has four equivalent C-F bonds in the equilibrium structure in T_d symmetry (**Figure 2**) to see if directional ejection of the fragment can be induced by asymmetric laser fields. The electronic configuration is $\ldots (1e)^4 (4t_2)^6 (1t_1)^6$ in the ground state. The highest-occupied MO (HOMO), $1t_1$, is triply degenerated (see **Figure 3**). We discuss dissociative ionization in ω-2ω intense laser fields:

$$CF_4 \rightarrow CF_3^+ + F + e^-. \quad (3)$$

The dissociative ionization has been subjected to single-photon (Brehm et al., 1974; Creasey et al., 1990; Hikosaka and Shigemasa, 2006; Tang et al., 2013; Larsen et al., 2018; Pertot et al., 2017) and electron impact (Hossen et al., 2018) studies. The process is characterized by the ultrashort lifetime (< 40 fs) (Pertot et al., 2017) on the repulsive PESs leading to the $CF_3^+ + F$ asymptote in both the ground and the first excited states of CF_4^+ as shown in **Figure 4**. The repulsive PESs imply that the CF_4 can serve as a unique benchmark to elucidate how the tunneling ionization of polyatomic molecules proceeds in intense laser fields because fragments can be produced by direct dissociation without additional interaction with the laser fields (Fujise et al., 2022).

The paper is organized as follows. We first describe the experimental setup for the three-dimensional momentum imaging of CF_3^+ fragment ions produced by dissociative ionization in **Eq. 3** in linearly polarized ω-2ω intense laser fields (50 fs, 1.4×10^{14} W/cm^2, 800 and 400 nm). Then, we present the experimental results on the asymmetry in the ejection of CF_3^+ and its dependence on the relative phase ϕ between the ω and 2ω laser fields. Finally, the obtained results are compared with theoretical predictions by the weak-field asymptotic theory (WFAT) (Tolstikhin et al., 2011) for tunneling ionization.

2 EXPERIMENT

The schematic of the experimental setup is shown in **Figure 1**. Details have been described previously (Endo et al., 2019). Briefly, the output from a Ti: Sapphire regenerative laser amplifier system (800 nm, 1 kHz, 50 fs) was introduced to an inline ω-2ω pulse generator. After generation of the second-order harmonics (400 nm, ~80 fs) by a type-I β-BBO crystal, the time delay between the ω and 2ω pulses was compensated by two birefringent α-BBO crystals. The relative phase between the two-color was controlled by a pair of fused silica wedge plates. The relative phase of the two-color laser pulses was stabilized by active feedback control of the wedge plate utilizing the 2ω-2ω interference spectrum. The polarization direction of the fundamental and second harmonic pulses was set parallel with each other by a true zero-order dual-wavelength plate and introduced into an ultrahigh vacuum chamber. The ω-2ω laser pulse was focused onto a diffusive molecular beam by a focusing mirror (f = 75 mm). Fragment ions generated by the interaction with ω-2ω intense laser fields were guided to a delay-line anode position-sensitive detector (PSD) by a static electric field. The three-dimensional momentum (p_X, p_Y, p_Z) of each fragment ion was obtained from the arrival position (Y, Z) at the detector and the time of flight (t). The kinetic energy release (KER) was calculated from the momentum of CF_3^+, $\mathbf{p}_{CF_3^+}$, where we assume the momentum conservation between CF_3^+ and the counterpart fragment F atom, $\mathbf{p}_F = -\mathbf{p}_{CF_3^+}$. Under this approximation, the KER is expressed as

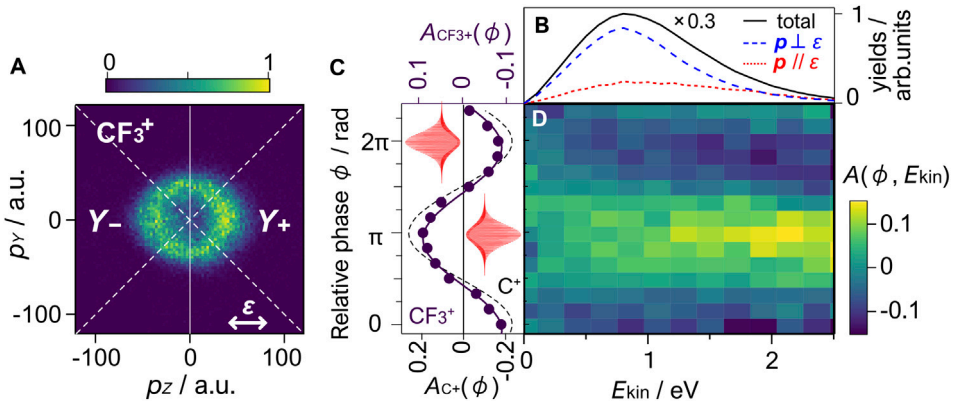

FIGURE 5 | (A) Momentum image of CF_3^+ fragment ions produced in ω-2ω intense laser fields (50 fs, 1.4×10^{14} W/cm^2, 800 and 400 nm), averaged over the relative phase ($0 \le \phi \le 2\pi$). The image is a slice of the three-dimensional ion momentum distribution in the *Y*-*Z* plane with a thickness of $|p_X| < 10$ a.u. The arrow represents the direction of the laser polarization. **(B)** Total kinetic energy release spectra of $CF_4^+ \rightarrow CF_3^+ + F$ (solid) plotted together with the parallel (dotted) and perpendicular (dashed) components, defined by the polar angles of $0^\circ \le \theta \le 20^\circ$ and $75^\circ \le \theta \le 90^\circ$, respectively. The total spectrum is multiplied by 0.3. **(C)** The asymmetry parameter $A_{CF_3^+}(\phi)$ for the CF_3^+ fragment ions with an acceptance angle of 45°(solid circle) and the results of the least-square fitting (solid line) (see text). The fitting results for the C^+ ion produced by the Coulomb explosion of CO (4 eV $\le E_{kin} \le$ 8 eV) are also plotted (dashed line). The laser pulse shapes at $\phi = 0$ and π are shown. **(D)** Two-dimensional plot of the asymmetry parameter $A(\phi, E_{kin})$ for CF_3^+.

$$E_{kin} = \frac{m_F + m_{CF_3^+}}{2m_F m_{CF_3^+}} |\mathbf{p}_{CF_3^+}|^2, \quad (4)$$

where $m_{CF_3^+}$ and m_F are the masses of the CF_3^+ fragment ions and F atoms, respectively.

The intensities of the laser fields were estimated to be $I_\omega = 1.15 \times 10^{14}$ W/cm^2 and $I_{2\omega} = 2.6 \times 10^{13}$ W/cm^2, respectively. The total field intensity is $I_{\omega+2\omega} = I_\omega + I_{2\omega} = 1.4 \times 10^{14}$ W/cm^2 with a ratio of $I_{2\omega}/I_\omega = 0.23$. A mixture of CF_4 and CO was used as the sample gas. The absolute phase difference ϕ between ω and 2ω pulses at the focal point was determined by the phase dependence of Coulomb explosion of CO, $CO \rightarrow C^+ + O^+ + 2e^-$, where C^+ is ejected more to the smaller amplitude side of the ω-2ω electric fields than to the opposite (Li et al., 2011).

3 RESULTS AND DISCUSSION

3.1 Fragment Momentum Distribution

Figure 5A shows the momentum image of CF_3^+ that dominates the time-of-flight spectrum, reflecting the repulsive nature of the PES of CF_4^+. The KER spectrum shows a broad single peak at E_{kin} = 0.8 eV as observed in the previous studies (Tang et al., 2013; Larsen et al., 2018; Hossen et al., 2018; Hikosaka and Shigemasa, 2006; Fujise et al., 2022). The CF_3^+ momentum image in **Figure 5A** shows an elliptic distribution. The peak momentum values along the *Z*-axis and *Y*-axis are 35 a.u. and 30 a.u., respectively, showing that CF_3^+ is emitted with a larger momentum along the laser polarization direction. **Figure 5B** shows the KER spectra obtained for parallel ($0^\circ \le \theta \le 20^\circ$) and perpendicular ($75^\circ \le \theta \le 90^\circ$) components to the laser polarization direction, where θ is the polar angle from the *Z*-axis. The parallel component shows a broader peak at 0.9 eV extending to a higher KER region than the perpendicular component. The perpendicular component has a sharper peak at 0.8 eV, indicating that different pathways contribute to the dissociative ionization. The previous electron impact study at an energy of 67 eV (Hossen et al., 2018) shows that contributions from five different molecular orbitals $1t_1$, $4t_2$, $1e$, $3t_2$, and $4a_1$ overlap within the peak. The KER spectrum associated with the ionization from HOMO ($1t_1$) exhibits a peak at ~0.9 eV, while a broader peak appears at a slightly higher energy region for HOMO-1 ($4t_2$). This suggests that both the X^2T_1 ground state and A^2T_2 first excited state contribute to the dissociative ionization in the ω-2ω intense laser fields, although it is difficult to estimate the relative contributions from these orbitals by the present experimental results. It is worth noting that the dissociation from the $1e$ HOMO-2 state may also contribute to the KER spectrum (Larsen et al., 2018) through internal conversion from the B^2E to the A^2T_2 state (Maier and Thommen, 1980).

3.2 Asymmetric Dissociative Ionization of CF_4

To understand how CF_4 responds to different shapes of the laser pulse, we focus on the spatial asymmetry in the fragment distribution. For a quantitative discussion, the asymmetry parameter,

$$A(\phi) = \frac{Y_+(\phi) - Y_-(\phi)}{Y_+(\phi) + Y_-(\phi)}, \quad (5)$$

is introduced, where Y_+ and Y_- represent the yields of ions with positive and negative momenta within a 45° acceptance angle along the laser polarization direction (*Z*-axis), respectively (see **Figure 5A**). **Figure 5C** plots the obtained asymmetry parameters for CF_3^+, $A_{CF_3^+}(\phi)$, together with those obtained for C^+ produced from the Coulomb explosion of CO used for the phase calibration. The asymmetry parameter shows a 2π periodic

dependence on the two-color relative phase. The least-squares fitting to $A(\phi) = A_0\cos(\phi\text{-}\phi_0)$ provides $A_0 = 0.09(1)$ and $\phi_0 = 0.9(1)\ \pi$, where numbers in the parentheses represent uncertainties. The results show that CF_3^+ prefers being emitted on the smaller electric field side of the asymmetric laser fields. In other words, the dissociative tunneling ionization is enhanced when the lager amplitude side of the ω-2ω electric fields points from C to F. **Figure 5D** shows the KER-resolved asymmetry parameter,

$$A(\phi, E_{\mathrm{kin}}) = \frac{Y_+(\phi, E_{\mathrm{kin}}) - Y_-(\phi, E_{\mathrm{kin}})}{Y_+(\phi, E_{\mathrm{kin}}) + Y_-(\phi, E_{\mathrm{kin}})}. \quad (6)$$

An increase in the asymmetry amplitude to $A_0 \sim 0.12$ is observed in higher KER region where contributions from the A^2T_2 state of CF_4^+ is observed. The maximum and minimum of the asymmetry parameter are seen at $\phi \sim \pi$ and 0, respectively, over the KER range investigated.

3.3 Comparison With Tunneling Ionization Theory

3.3.1 Tunneling Ionization Rates

Theoretical calculations of the tunneling ionization rate of CF_4 were carried out by WFAT (Tolstikhin et al., 2011). The tunneling ionization rate is expressed as (Madsen et al., 2012)

$$\Gamma(\beta, \gamma) = |G_{00}(\beta, \gamma)|^2 W_{00}(F). \quad (7)$$

The structure factor $G_{00}(\beta, \gamma)$ describes the dependence on the molecular orientation relative to the laser electric field F defined by the Euler angles (α, β, γ) (Zare, 1988). The field factor $W_{00}(F)$ is given as

$$W_{00}(F) = \frac{\varkappa}{2}\left(\frac{4\varkappa^2}{F}\right)^{2/\varkappa-1} \exp\left(-\frac{2\varkappa^3}{3F}\right), \quad (8)$$

which defines the dependence on the field strength F. Here, $\varkappa = \sqrt{-2E_0}$, with E_0 being the energy of the molecular orbital from which the electron is ionized, and the subscript 00 refers to the dominant ionization channel (Tolstikhin et al., 2011).

The HOMO ($1t_1$) and HOMO-1 ($4t_2$) of CF_4 are both triply degenerate (**Figure 3**). The Stark interaction with the ionizing field removes the degeneracy. Tunneling ionization occurs from eigenorbitals of the operator $-(\boldsymbol{\mu}\cdot\boldsymbol{F})$ within each degenerate subspace, where $\boldsymbol{\mu}$ is the electric dipole moment of the considered orbital (Kraus et al., 2015). We denote these eigenorbitals as ϕ_A, ϕ_B, and ϕ_C. The three eigenorbitals are the particular linear combinations of the three degenerate HOMOs shown in **Figure 3**, which diagonalize the Stark term $(\boldsymbol{\mu}\cdot\boldsymbol{F})$. The structure factors $G_{00}(\beta, \gamma)$ incorporating the effect of the dipole for the eigenorbitals are calculated using the integral representation of the WFAT (Dnestryan and Tolstikhin, 2016; Madsen et al., 2017; Dnestryan et al., 2018) implemented by means of the GAMESS package with a polarization consistent basis set at the pc-4 level (Jensen, 2001).

Figures 6A–C show the squared norms of the structure factors $|G_{00}(\beta, \gamma)|^2$ of the three eigenorbitals, ϕ_A, ϕ_B, and ϕ_C, in the subspace of HOMO ($E_0 = -18.66$ eV), where the orbitals are labeled with A, B, and C in the ascending order of the dipole, $\mu_A < \mu_B < \mu_C$. The orbital energy in the field to the first order is given as

$$E_{0,i}(\boldsymbol{F}) = E_0 - \boldsymbol{\mu}_i \cdot \boldsymbol{F}, \quad (9)$$

where i = A,B,C. **Figure 7** shows the energy of eigenorbitals calculated using **Eq. 9** at four different molecular orientations with respect to F. The structure factors for HOMO in **Figures 6A–C** show that the largest contribution to the tunneling ionization comes from eigenorbital ϕ_B because the field factor $W_{00}(F)$ is common for ϕ_A, ϕ_B, and ϕ_C (see **Eq. 7**). Each orbital has nodes along the C-F axis, which appear as the minima in the respective structure factors. The nodes remain visible in the sum of $|G_{00}(\beta, \gamma)|^2$ in **Figure 6D**.

The squared norms of the structure factors $|G_{00}(\beta, \gamma)|^2$ of HOMO-1 ($E_0 = -19.44$ eV) are shown in **Figures 6E–H**. The eigenorbital ϕ_A having the highest energy among the three orbitals has the largest contributions to the sum in **Figure 6H**. **Figure 6H** shows that the tunneling ionization is enhanced by the electric field pointing from F to C when the three degenerated eigenorbitals are equally populated. Because eigenenergy $E_{0,A}$ of ϕ_A at $(\beta, \gamma) = (124^\circ, 314^\circ)$ is slightly smaller than that at $(\beta, \gamma) = (54^\circ, 134^\circ)$, the large structure factors for the former orientation indicate that the shape of the molecular orbital is more important in determining the tunneling rate in the present case than the increase in the effective ionization potential by the Stark interaction with the dipole moment.

3.3.2 Fragment Angular Distribution

If the breaking of each of the four C-F bonds after ionization occurs with an equal probability, the angular distribution of the F fragment in the laboratory frame can be expressed as follows (Zare, 1988):

$$P(\theta_s, \phi_s) = \int_0^{2\pi} \mathrm{d}\alpha \int_0^{\pi} \sin\beta \mathrm{d}\beta \int_0^{2\pi} \mathrm{d}\gamma P_{\mathrm{mol}}(\alpha, \beta, \gamma) f(\theta_m, \phi_m), \quad (10)$$

where (θ_s, ϕ_s) and (θ_m, ϕ_m) are the spherical angles with respect to the laboratory and molecular frame, respectively, and $f(\theta_m, \phi_m)$ is the angular distribution of the fragment ion in the molecular frame. The orientation distribution of the molecular ion formed in the ω-2ω laser fields in the laboratory frame may be expressed as

$$P_{\mathrm{mol}}(\alpha, \beta, \gamma) = \frac{1}{8\pi^2}\left\{1 - \exp\left[-\int_{-\infty}^{+\infty} \Gamma_s(\alpha, \beta, \gamma, F(t))\mathrm{d}t\right]\right\}, \quad (11)$$

where $\Gamma_s(\alpha, \beta, \gamma, F(t))$ represents the tunneling rate in the ω-2ω laser field $F(t)$ of **Eq. 2** for molecular orientation defined by the Euler angles (α, β, γ) relative to the Z-axis of the laboratory frame (see **Figure 2**). It can be expressed by $|G_{00}(\beta, \gamma)|^2$ and $W_{00}(F)$ as follows:

$$\Gamma_s(\alpha, \beta, \gamma, F(t)) = \begin{cases} |G_{00}(\beta, \gamma)|^2 W_{00}(|F(t)|) & (F(t) \geq 0) \\ |G_{00}(\pi - \beta, \gamma + \pi)|^2 W_{00}(|F(t)|) & (F(t) < 0) \end{cases}. \quad (12)$$

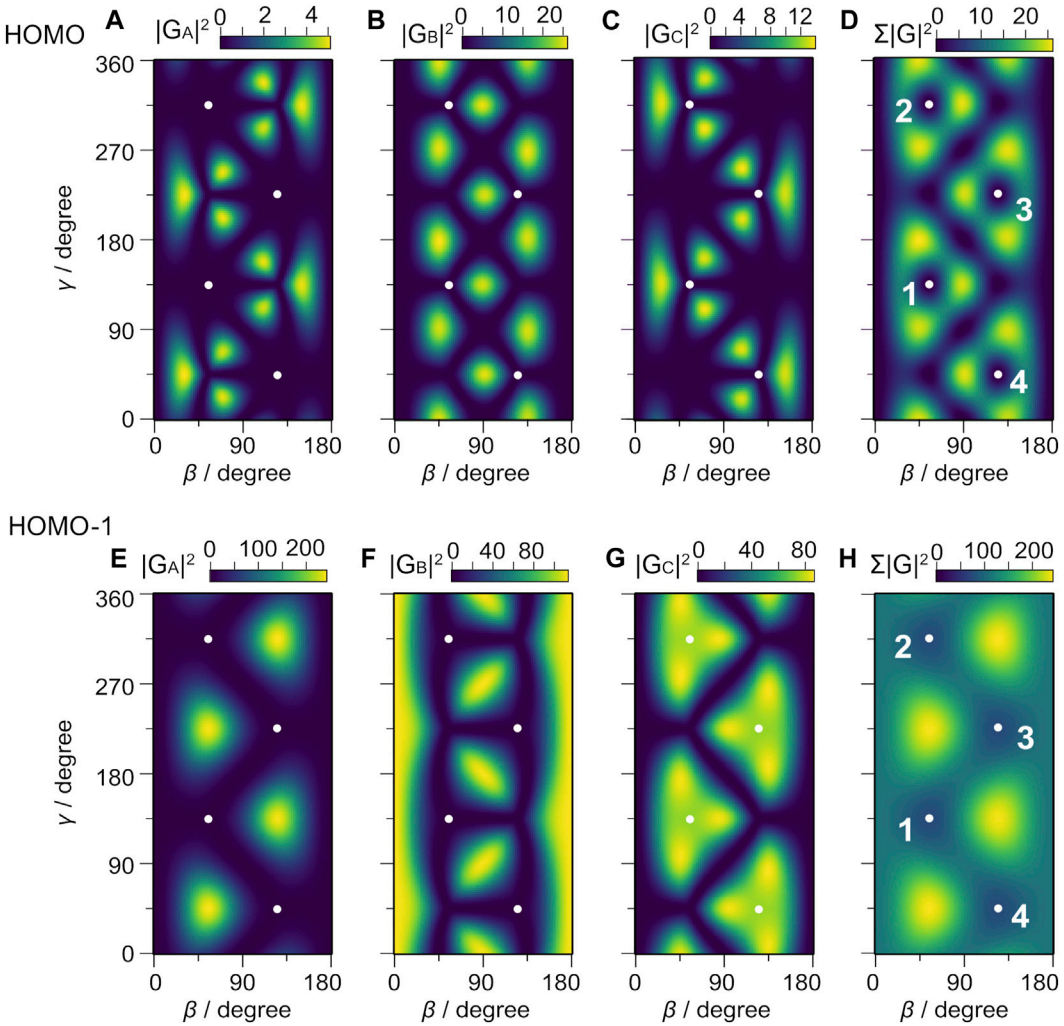

FIGURE 6 | Structure factors of eigenorbitals, **(A)** $|G_A|^2$, **(B)** $|G_B|^2$, **(C)** $|G_C|^2$, and **(D)** the sum, $\Sigma|G|^2 = |G_A|^2 + |G_B|^2 + |G_C|^2$ for HOMO, and **(E)** $|G_A|^2$, **(F)** $|G_B|^2$, **(G)** $|G_C|^2$ and **(H)** $\Sigma|G|^2$ for HOMO-1. The dots represent the Euler angles (β, γ) at which one of the C-F axes points to the Z direction. The numbers attached to the dots in panels **(D,H)** represent the labels of the respective F atoms in **Figure 2**. Note the difference in the scaling of the color bars in **(A–H)**.

When the ionization probability is sufficiently smaller than unity, **Eq. 11** reduces to

$$P_{\mathrm{mol}}(\alpha,\beta,\gamma) = \frac{1}{8\pi^2}\int_{-\infty}^{+\infty}\Gamma_s(\alpha,\beta,\gamma,F(t))\mathrm{d}t. \tag{13}$$

The angular distribution $P_{\mathrm{mol}}(\alpha, \beta, \gamma)$ can be expanded by the rotation matrices $D^k_{q'q}(R)$ as follows:

$$P_{\mathrm{mol}}(\alpha,\beta,\gamma) = \frac{1}{8\pi^2}\sum_{k,q,q'} a^k_{q'q} D^{k*}_{q'q}(\alpha,\beta,\gamma). \tag{14}$$

Here, the coefficients $a^k_{q'q}$ are given as follows:

$$a^k_{q'q} = (2k+1)\int P_{\mathrm{mol}}(\alpha,\beta,\gamma) D^k_{q'q}(R)\mathrm{d}\Omega. \tag{15}$$

The angular distribution of the fragment ion can be expressed using the spherical harmonics $Y_{jm}(\theta_m, \phi_m)$:

$$f(\theta_m,\phi_m) = \sum_{j,m} b_{jm} Y_{jm}(\theta_m,\phi_m), \tag{16}$$

$$b_{jm} = \int_0^{2\pi}\mathrm{d}\phi_m\int_0^{\pi}\sin\theta_m \mathrm{d}\theta_m Y^*_{jm}(\theta_m,\phi_m) f(\theta_m,\phi_m). \tag{17}$$

Thus, we have

$$P(\theta_s,\phi_s) = \sum_{k,q,q'}\frac{a^k_{q'q} b_{kq}}{2k+1} Y_{kq'}(\theta_s,\phi_s). \tag{18}$$

Under the axial recoil approximation, the angle distribution $f(\theta_m, \phi_m)$ may be expressed as follows:

$$f(\theta_m,\phi_m) = \frac{1}{\sin\theta_m}\delta(\theta_m-\theta^0_m)\delta(\phi_m-\phi^0_m), \tag{19}$$

with $(\theta^0_m, \phi^0_m) = (54.7^\circ, 45^\circ)$ for CF_4 in T_d symmetry. By substituting to **Eq. 17**, we have

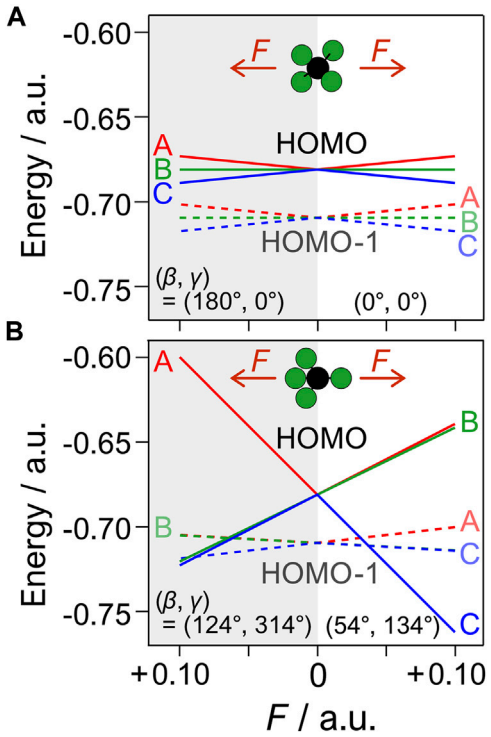

FIGURE 7 | Stark shifted energies of $E_{0,i}(F)$ of eigenorbitals, ϕ_i (i = A, B, C), of HOMO (solid line) and HOMO-1 (dashed line) as a function of the static field F (see **Eq. 9**) at four different molecular orientations with respect to F, defined by the Euler angles (β, γ) in **Figure 2**. **(A)** The electric field is parallel to the molecular principal axis (C_2), i.e., (β, γ) = (0°, 0°) (right) and (180°, 0°) (left). **(B)** The same as **(A)** but for (β, γ) = (54°,134°) (right) and (124°, 314°) (left), where the electric field is almost parallel to one of the C-F axes.

$$b_{jm} = Y^*_{jm}(\theta^0_m, \phi^0_m) = (-1)^m Y_{j-m}(\theta^0_m, \phi^0_m), \tag{20}$$

from which we obtain an expression for the fragment angular distribution as follows:

$$P(\theta_s, \phi_s) = P(\theta_s) = \frac{1}{\sqrt{4\pi}} \sum_k c_k P_k(\cos\theta_s), \tag{21}$$

$$c_k = \frac{1}{\sqrt{2k+1}} \sum_q a^k_{0q} Y^*_{kq}(\theta^0_m, \phi^0_m). \tag{22}$$

Figure 8 shows the fragment angular distributions obtained for the relative phase ϕ = 0 of the ω - 2ω pulse ($I_{\omega+2\omega}$ = 1.4 × 10^{14} W/cm^2 and $I_{2\omega}/I_\omega$ = 0.23). The calculated fragment yields for HOMO-1 is larger than that of HOMO under the present experimental conditions (F_ω = 0.057 a.u. and $F_{2\omega}$ = 0.027 a.u.).

This is attributed to the large structure factor $|G_{00}|^2$ for HOMO-1 (**Figure 6H**), which is about 10 times larger than $|G_{00}|^2$ for HOMO (**Figure 6D**), because of the small difference between the ionization potentials of these orbitals (~1 eV) giving rise to the relatively small field factor ratio of $W_{00}(1t_1)/W_{00}(4t_2)$ ~ 3. The angular distribution calculated for each HOMO exhibits characteristic structures associated with the nodes of the molecular orbitals. The total fragment distribution carries the nodal pattern with a larger ionization probability on the larger amplitude side of the ω-2ω laser fields. In contrast, the angular distribution of HOMO-1 is more directional along the laser polarization direction, consistent with the fragment ion image and the KER spectra in **Figures 5A,B**, where the ionization from HOMO-1 contributes more to the parallel component than to the perpendicular one.

3.3.3 Asymmetry Parameter

The yields of the F fragment in a finite acceptance angle θ_0 around 0° and 180° can be expressed as follows:

$$Y^{\theta_0}_{+}(\phi) = 2\pi \int_0^{\theta_0} P(\theta_s) \sin\theta_s d\theta_s, \tag{23}$$

$$Y^{\theta_0}_{-}(\phi) = 2\pi \int_{\pi-\theta_0}^{\pi} P(\theta_s) \sin\theta_s d\theta_s. \tag{24}$$

The asymmetry parameters defined by **Eq. 5** are calculated using **Eqs 23**, **24**, where θ_0 = 45° compared with the experimental results. The asymmetry parameter $A_F(\phi)$ thus obtained for HOMO shows a clear dependence on the relative phase ϕ between the ω and 2ω laser fields. The asymmetry parameter for HOMO (**Figure 9A**) is positive at ϕ = 0, showing that tunneling ionization is more efficient when the larger amplitude side of the laser fields points from C to F. In contrast, the parameter for HOMO-1 exhibits the opposite dependence with negative values at ϕ = 0. The difference originates essentially from the shape of the eigenorbitals dominating the tunneling ionization of the respective MOs.

Figure 9B plots the experimental asymmetry parameter $A_F(\phi)$ for the counterpart fragment F produced by the dissociative ionization (**Eq. 3**), which is obtained from the asymmetry parameter for CF_3^+ by $A_F(\phi) = -A_{CF_3^+}(\phi)$. It is compared with the corresponding asymmetry parameter calculated with the contributions from the two orbitals, where the angular distribution is given as $P(\theta_s) = P_{HOMO}(\theta_s) + P_{HOMO\text{-}1}(\theta_s)$. The obtained amplitude of A_0 = 0.1 is slightly larger than the experimental results. The small experimental amplitude might be attributed to the contribution from HOMO-2 (1e), located ~1.4 eV below the HOMO-1. The B^2E state of CF_4^+ produced by the tunneling ionization from 1e has a lifetime of 10^{-10}–10^{-12} s (Maier and Thommen, 1980). This lifetime is longer than or comparable with the molecular rotational periods and could form an isotropic fragment distribution, which reduces the asymmetry of the fragmentation. **Figure 9B** plots the asymmetry parameter $A_F(\phi)$ obtained at a higher field intensity 3.0 × 10^{14} W/cm^2 with a similar intensity ratio of $I_{2\omega}/I_\omega$ = 0.25. The increase in the field intensity resulted in a small amplitude A_0 ~ 0.04, while the amplitude of the calculated results remained essentially the same. Because the relative contribution from the B^2E state is expected to increase by an increase in the field intensity, the experimental results support the involvement of the B^2E state in the dissociative ionization.

Interestingly, the calculated asymmetry parameter in **Figure 9B** has an opposite phase dependence to the experimental results, showing that the dissociative tunneling ionization of CF_4 in the ω-2ω laser fields cannot be explained by the angular distribution of the tunneling ionization from

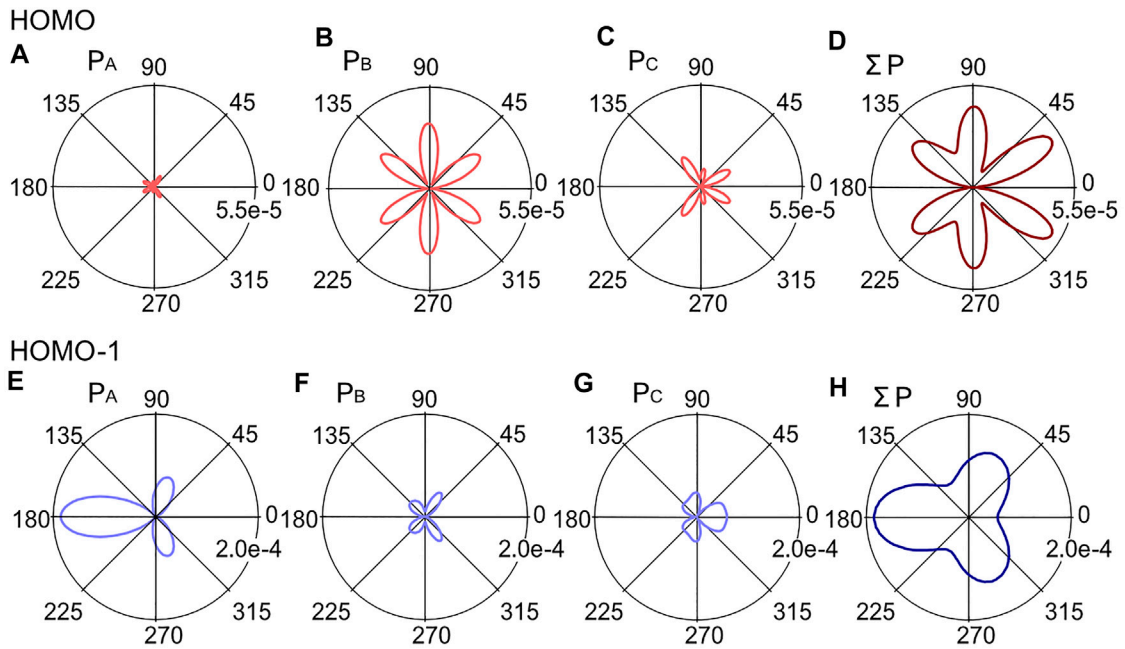

FIGURE 8 | Angular distributions $P(\theta_s)$ calculated for the eigenorbitals, ϕ_A, ϕ_B, and ϕ_C, in the ω-2ω laser field with the relative phase $\phi = 0$, **(A)** $P_A(\theta_s)$, **(B)** $P_B(\theta_s)$, **(C)** $P_C(\theta_s)$, and **(D)** the sum $\Sigma P(\theta_s)$ for HOMO and **(E)** $P_A(\theta_s)$, **(F)** $P_B(\theta_s)$, **(G)** $P_C(\theta_s)$ and **(H)** $\Sigma P(\theta_s)$, for HOMO-1. Note the difference in the scaling of the polar plots for HOMO and HOMO-1.

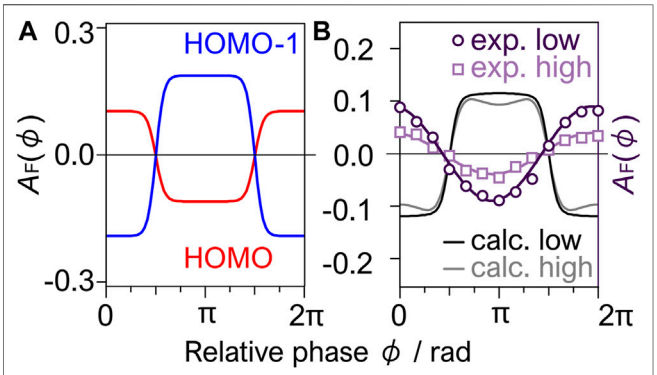

FIGURE 9 | (A) Phase dependence of the asymmetry parameter $A(\phi)$ calculated for HOMO and HOMO-1 with the acceptance angle of $\theta_0 = 45°$. **(B)** Total asymmetry parameter compared with the experimental parameter for F fragment, $A_F(\phi)$, calculated at $I_{\omega+2\omega} = 1.4 \times 10^{14}$ W/cm^2 (solid) and 3.0×10^{14} W/cm^2 (gray), in comparison with the corresponding experimental results (circle and square, respectively).

the HOMO and HOMO-1 alone, although the F (or CF_3^+) fragments are promptly ejected on the repulsive potentials of the X^2T_1 and A^2T_2 states after the tunneling ionization (**Figure 4**). The present experimental results show a marked contrast to those obtained by recent studies on the dissociative ionization of CF_4 in circularly polarized laser fields (35 fs, 0.8×10^{14} W/cm^2, 1,035 nm) (Fujise et al., 2022). The recoil-frame photoelectron angular distribution (RFPAD) showed that the dissociative tunneling ionization occurs more efficiently when the electric field points from F to C than the opposite, which is consistent with the prediction by WFAT for the tunneling ionization (see also **Figure 8**).

Previous studies on spatially oriented OCS showed that the tunneling ionization yields exhibit different angular dependence in linearly polarized and circularly polarized laser fields (Holmegaard et al., 2010; Hansen et al., 2012) as in the present case, where the tunneling ionization is enhanced at different directions of the applied electric fields in the molecular frame. For circularly polarized fields, a significant enhancement of tunneling ionization was observed when the electric fields were applied from C to S along the molecular axis, while the linearly polarized fields favor the tunneling ionization from the direction perpendicular to the axis. The discrepancy was discussed in terms of electron rescattering and the involvement of electronic excitation (Hansen et al., 2012), as well as orbital modification (Murray et al., 2010) and multielectron effects (Majety and Scrinzi, 2015) in the ionization process. These effects can, in principle, be involved in the present case of CF_4 to explain the deviation between the experimental and theoretical results in **Figure 9B**. Furthermore, **Figure 7** suggests that the energy shifts of eigenorbitals formed by the Stark interaction becomes large enough to induce mixing between HOMO and HOMO-1, for example, at a field intensity $F \geq 0.06$ a.u. in the molecular orientation in **Figure 7B**. This would result in additional polarization (field-induced deformation) of the ionizing orbitals, which affects the ionization rate (Matsui et al., 2021) but is not considered in the calculation of the structure factors in **Figure 6**.

Because the directional ejection of the fragments involves both ionization and fragmentation, post-ionization interaction with the laser fields (Endo et al., 2019; Endo et al., 2022) is

another important factor to consider. The post-ionization interaction in ω-2ω laser fields has been extensively studied with H_2^+ (Ray et al., 2009; Wanie et al., 2015). The dissociative ionization shows a clear dependence on the relative phase ϕ. The H^+ ejection direction is determined by the quantum interference between the pathways associated with excitation and deexcitation between the $1s\sigma_g$ and $2p\sigma_u$ states of H_2^+ by absorption or emission of ω and 2ω photons. This results in the spatial asymmetry of H^+ ejection dependent on both phase ϕ and KER. The quantum interference effect can also manifest itself in circularly polarized laser fields when the tunneling electron is detected in coincidence with H^+ (Wu et al., 2013). It appears as the distortion of the molecular-frame photoelectron angular distribution (MFPAD). As for CF_4, the RFPADs recorded for the dissociative ionization in **Eq. 3** in circularly polarized fields exhibited clear dependences on both the helicity of circularly polarized laser fields and the KER [1]. The observed results are interpreted in terms of the laser-induced coupling between the electronic states, depending on the phase of the rotating electric fields in the molecular frame. The coupling between the ground state X^2T_1 and the excited state A^2T_2 through non-adiabatic population transfer in the alternating laser electric fields was suggested as a possible dynamics contributing to the helicity dependence. In the present case of the two-color laser fields consisting of 800 and 400 nm for ω and 2ω, the energy differences between the states and the A^2T_2 and B^2E states are close to the photon energy of $h\nu$ = 1.5 and 3.1 eV of the present ω and 2ω fields (see **Figure 4**), which further facilitates such coupling to modify the asymmetry of the fragmentation through quantum interferences.

4 SUMMARY

In the present study, we investigated the directional fragment ejection of CF_4 in dissociative ionization, $CF_4 \rightarrow CF_3^+ + F + e^-$, in linearly polarized ω-2ω ultrashort intense laser fields (1.4×10^{14} W/cm^2, 800 and 400 nm) by three-dimensional ion momentum imaging. The CF_3^+ fragment distribution exhibited a clear dependence on the relative phase ϕ between the ω and 2ω laser fields, showing that the CF_3^+ ions tend to be ejected to smaller electric field sides of the two-color laser fields. The observed results indicated that the asymmetric ejection of the CF_3^+ ion or the F fragment can be manipulated by the relative phase of the ω-2ω intense laser fields. To understand the mechanism of the directional fragment ejection, the tunneling ionization rates were calculated by the weak-field asymptotic theory (WFAT) incorporating the Stark interaction in the triply degenerated orbitals of HOMO and HOMO-1. It was shown that the contributions from the HOMO-1 ($4t_2$) are even larger than those from HOMO ($1t_1$). The inverted order is attributed to the large structure factor of HOMO-1, which is governed essentially by the shape of the MO. The observed momentum distribution of CF_3^+ and the KER spectrum supported that both the X^1T_1 and A^2T_2 states contribute to the dissociative ionization of CF_4 in the ω-2ω intense laser fields.

In contrast, WFAT showed that the ionization yield sum becomes larger when the electric field points from F to C along the one of the C-F axis to predict a phase-dependent asymmetry parameter $A(\phi)$ being π out-of-phase to the experimental one. The difference between experimental and theoretical results could be attributed to additional distortion of molecular orbitals by mixing between HOMO and HOMO-1, as well as to the other processes proposed in the previous studies. The post-ionization process is another possible source of different phase dependence. The direct coupling between the electronic states of CF_4^+ by non-adiabatic transitions between the orbitals would cause constructive and destructive interference of the dissociating nuclear wavepackets to make the four C-F bonds inequivalent in dissociation. The present study demonstrated the feasibility of applying strong-field coherent control of directional fragment ejection to a symmetric polyatomic molecule in T_d symmetry. Several factors need to be considered to fully understand the selective breaking of C-F bonds in the dissociative tunneling ionization, even though ultrafast dissociation occurs on the repulsive potential surfaces after the ionization.

DATA AVAILABILITY STATEMENT

The original contributions presented in the study are included in the article/Supplementary Material. Further inquiries can be directed to the corresponding author.

AUTHOR CONTRIBUTIONS

HH, TW, and AM performed experiments and data analysis. TM, LBM, FJ, OIT, HH, and AH carried out theoretical calculations and simulations. AH conceived and directed the project, supervised the experiments, and analyzed data. HH and AH wrote the original draft. All authors contributed to the discussions of the results and to the production of the manuscript.

FUNDING

This work was supported by JSPS KAKENHI (Grant nos. JP19H00887, JP16H04029, and JP21K18929), MEXT Quantum Leap Flagship Program (MEXT Q-LEAP) (Grant no. JPMXS0118068681), and World Research Unit (B-1) of Reaction Infography (R-ing) at Nagoya University. This work was financially supported by JST SPRING, Grant Number JPMJSP2125. HH would like to take this opportunity to thank the "Interdisciplinary Frontier Next-Generation Researcher Program of the Tokai Higher Education and Research System." OIT was supported by the Ministry of Science and Higher Education of the Russian Federation (No.FSMG-2021-0005).

REFERENCES

Assion, A., Baumert, T., Bergt, M., Brixner, T., Kiefer, B., Seyfried, V., et al. (1998). Control of Chemical Reactions by Feedback-Optimized Phase-Shaped Femtosecond Laser Pulses. *Science* 282, 919–922. doi:10.1126/science.282.5390.919

Bardeen, C. J., Yakovlev, V. V., Wilson, K. R., Carpenter, S. D., Weber, P. M., and Warren, W. S. (1997). Feedback Quantum Control of Molecular Electronic Population Transfer. *Chem. Phys. Lett.* 280, 151–158. doi:10.1016/s0009-2614(97)01081-6

Bartels, R., Backus, S., Christov, I., Kapteyn, H., and Murnane, M. (2000). Attosecond Time-Scale Feedback Control of Coherent X-ray Generation. *Chem. Phys.* 267, 277. doi:10.1016/s0301-0104(01)00213-0

Brehm, B., Frey, R., Küstler, A., and Eland, J. (1974). Kinetic Energy Release in Ion Fragmentation: N_2O^+, COS^+ and CF_4^+ Decays. *Int. J. Mass Spectrom. Ion Phys.* 13, 251–260. doi:10.1016/0020-7381(74)80029-x

Chan, H.-S., Hsieh, Z.-M., Liang, W.-H., Kung, A. H., Lee, C.-K., Lai, C.-J., et al. (2011). Synthesis and Measurement of Ultrafast Waveforms from Five Discrete Optical Harmonics. *Science* 331, 6021. doi:10.1126/science.1198397

Creasey, J. C., Lambert, I. R., Tuckett, R. P., Codling, K., Frasinski, L. J., Hatherly, P. A., et al. (1990). Nonradiative Decay Pathways of Electronic States of Group IV Tetrafluoro and Tetrachloro Molecular Ions Studied with Synchrotron Radiation. *J. Chem. Phys.* 93, 3295–3306. doi:10.1063/1.458810

Dnestryan, A. I., and Tolstikhin, O. I. (2016). Integral-Equation Approach to the Weak-Field Asymptotic Theory of Tunneling Ionization. *Phys. Rev. A* 93, 033412. doi:10.1103/physreva.93.033412

Dnestryan, A. I., Tolstikhin, O. I., Madsen, L. B., and Jensen, F. (2018). Structure Factors for Tunneling Ionization Rates of Molecules: General Grid-Based Methodology and Convergence Studies. *J. Chem. Phys.* 149, 164107. doi:10.1063/1.5046902

Eickhoff, K., Englert, L., Bayer, T., and Wollenhaupt, M. (2021). Multichromatic Polarization-Controlled Pulse Sequences for Coherent Control of Multiphoton Ionization. *Front. Phys.* 9, 675258. doi:10.3389/fphy.2021.675258

Endo, T., Fujise, H., Hasegawa, H., Matsuda, A., Fushitani, M., Tolstikhin, O. I., et al. (2019). Angle Dependence of Dissociative Tunneling Ionization of NO in Asymmetric Two-Color Intense Laser Fields. *Phys. Rev. A* 100, 053422. doi:10.1103/physreva.100.053422

Endo, T., Fujise, H., Kawachi, Y., Ishihara, A., Matsuda, A., Fushitani, M., et al. (2017). Selective Bond Breaking of CO_2 in Phase-Locked Two-Color Intense Laser Fields: Laser Field Intensity Dependence. *Phys. Chem. Chem. Phys.* 19, 3550–3556. doi:10.1039/c6cp07471e

Endo, T., Fujise, H., Matsuda, A., Fushitani, M., Kono, H., and Hishikawa, A. (2016). Coincidence Momentum Imaging of Asymmetric Coulomb Explosion of CO_2 in Phase-Locked Two-Color Intense Laser fields. *J. Electron Spectrosc. Relat. Phenomena* 207, 50–54. doi:10.1016/j.elspec.2015.12.010

Endo, T., Ziems, K. M., Richter, M., Froebel, F. G., Hishikawa, A., and Gräfe, S. (2022). Post-Ionization Dynamics of Polar Molecules in Asymmetric Laser Fields. *Front. Chem.*. doi:10.3389/fchem.2022.859750

Hansen, J. L., Holmegaard, L., Nielsen, J. H., Stapelfeldt, H., Dimitrovski, D., and Madsen, L. B. (2012). Orientation-Dependent Ionization Yields from strong-field Ionization of Fixed-In-Space Linear and Asymmetric Top Molecules. *J. Phys. B: At. Mol. Opt. Phys.* 45, 015101. doi:10.1088/0953-4075/45/1/015101

Hikosaka, Y., and Shigemasa, E. (2006). Anisotropic Fragment Emission on Valence Photoionization of CF_4. *J. Electron Spectrosc. Relat. Phenomena* 152, 29–32. doi:10.1016/j.elspec.2006.02.005

Hishikawa, A., Matsuda, A., and Fushitani, M. (2020). Ultrafast Reaction Imaging and Control by Ultrashort Intense Laser Pulses. *Bull. Chem. Soc. Jpn.* 93, 1293–1304. doi:10.1246/bcsj.20200158

Holmegaard, L., Hansen, J. L., Kalhøj, L., Kragh, S. L., Stapelfeldt, H., Filsinger, F., et al. (2010). Photoelectron Angular Distributions from Strong-Field Ionization of Oriented Molecules. *Nat. Phys.* 6, 428–432. doi:10.1038/nphys1666

Hossen, K., Ren, X., Wang, E., Kumar, S. V. K., and Dorn, A. (2018). An (e, 2e + ion) Study of Electron-Impact Ionization and Fragmentation of Tetrafluoromethane at Low Energies. *Eur. Phys. J. D* 72, 43. doi:10.1140/epjd/e2017-80665-8

Fujise, H., Uemura, M., Hasegawa, H., Ikeya, D., Matsuda, A., Morishita, T., et al. (2022). Helicity-Dependent Dissociative Tunneling Ionization of CF_4 in Multicycle Circularly Polarized Intense Laser Fields. *Phys. Chem. Chem. Phys.*. doi:10.1039/d1cp05858d

Jensen, F. (2001). Polarization Consistent Basis Sets: Principles. *J. Chem. Phys.* 115, 9113–9125. doi:10.1063/1.1413524

Kechaoglou, E., Kaziannis, S., and Kosmidis, C. (2019). Controlling Intramolecular Hydrogen Migration by Asymmetric Laser Fields: the Water Case. *Phys. Chem. Chem. Phys.* 21, 11259–11265. doi:10.1039/c9cp01470e

Kraus, P. M., Tolstikhin, O. I., Baykusheva, D., Rupenyan, A., Schneider, J., Bisgaard, C. Z., et al. (2015). Observation of Laser-Induced Electronic Structure in Oriented Polyatomic Molecules. *Nat. Commun.* 6, 7039. doi:10.1038/ncomms8039

Larsen, K. A., Trevisan, C. S., Lucchese, R. R., Heck, S., Iskandar, W., Champenois, E., et al. (2018). Resonance Signatures in the Body-Frame Valence Photoionization of CF_4. *Phys. Chem. Chem. Phys.* 20, 21075–21084. doi:10.1039/c8cp03637c

Levis, R. J., Menkir, G. M., and Rabitz, H. (2001). Selective Bond Dissociation and Rearrangement with Optimally Tailored, Strong-Field Laser Pulses. *Science* 292, 709–713. doi:10.1126/science.1059133

Levis, R. J., and Rabitz, H. A. (2002). Closing the Loop on Bond Selective Chemistry Using Tailored strong Field Laser Pulses. *J. Phys. Chem. A* 106, 6427–6444. doi:10.1021/jp0134906

Li, H., Ray, D., De, S., Znakovskaya, I., Cao, W., Laurent, G., et al. (2011). Orientation Dependence of the Ionization of CO and NO in an Intense Femtosecond Two-Color Laser Field. *Phys. Rev. A* 84, 043429. doi:10.1103/physreva.84.043429

Madsen, L. B., Jensen, F., Dnestryan, A. I., and Tolstikhin, O. I. (2017). Structure Factors for Tunneling Ionization Rates of Molecules: General Hartree-Fock-Based Integral Representation. *Phys. Rev. A* 96, 013423. doi:10.1103/physreva.96.013423

Madsen, L. B., Tolstikhin, O. I., and Morishita, T. (2012). Application of the Weak-Field Asymptotic Theory to the Analysis of Tunneling Ionization of Linear Molecules. *Phys. Rev. A* 85, 053404. doi:10.1103/physreva.85.053404

Maier, J. P., and Thommen, F. (1980). Non-radiative Decay of Electronically Excited CF_4^+ (B^2E) and $CFCl_3^+$ (D^2E) Cations in the Gaseous Phase. *Chem. Phys. Lett.* 78, 54. doi:10.1016/0009-2614(81)85550-9

Majety, V. P., and Scrinzi, A. (2015). Static Field Ionization Rates for Multi-Electron Atoms and Small Molecules. *J. Phys. B: At. Mol. Opt. Phys.* 48, 245603. doi:10.1088/0953-4075/48/24/245603

Manzoni, C., Mücke, O. D., Cirmi, G., Fang, S., Moses, J., Huang, S., et al. (2015). Coherent Pulse Synthesis: Towards Sub-Cycle Optical Waveforms. *Laser Photon. Rev.* 9, 129–171. doi:10.1002/lpor.201400181

Matsui, H., Tolstikhin, O. I., and Morishita, T. (2021). Weak-Field Asymptotic Theory of Tunneling Ionization of the Hydrogen Molecule Including Core Polarization, Spectator Nucleus, and Internuclear Motion Effects. *Phys. Rev. A* 103, 033102. doi:10.1103/physreva.103.033102

Murray, R., Spanner, M., Patchkovskii, S., and Ivanov, M. Y. (2010). Tunnel Ionization of Molecules and Orbital Imaging. *Phys. Rev. Lett.* 106, 173001. doi:10.1103/physrevlett.106.173001

Neyra, E., Videla, F., Ciappina, M. F., Pérez-Hernández, J. A., Roso, L., and Torchia, G. A. (2018). Synthesis of Ultrashort Laser Pulses for High-Order Harmonic Generation. *Phys. Rev. A* 98, 013403. doi:10.1103/physreva.98.013403

Ohmura, H., Ito, F., and Tachiya, M. (2006a). Phase-Sensitive Molecular Ionization Induced by a Phase-Controlled Two-Color Laser Field in Methyl Halides. *Phys. Rev. A* 74, 043410. doi:10.1103/physreva.74.043410

Ohmura, H., Saito, N., and Morishita, T. (2014). Molecular Tunneling Ionization of the Carbonyl Sulfide Molecule by Double-Frequency Phase-Controlled Laser fields. *Phys. Rev. A* 89, 013405. doi:10.1103/physreva.89.013405

Ohmura, H., Saito, N., and Morishita, T. (2011). Quantum Control of Molecular Tunneling Ionization in the Spatiotemporal Domain. *Phys. Rev. A* 83, 063407. doi:10.1103/physreva.83.063407

Ohmura, H., and Saito, N. (2020). Sub-Optical-Cycle Attosecond Control of Molecular Ionization by Using Fourier-Synthesized Laser Fields. *Phys. Rev. A* 101, 043419. doi:10.1103/physreva.101.043419

Ohmura, H., Saito, N., and Tachiya, M. (2006b). Selective Ionization of Oriented Nonpolar Molecules with Asymmetric Structure by Phase-Controlled Two-Color Laser Fields. *Phys. Rev. Lett.* 96, 173001. doi:10.1103/physrevlett.96.173001

Ohmura, S., Ohmura, H., Kato, T., and Kono, H. (2021). Manipulation of Multielectron Dynamics of Molecules by Fourier-Synthesized Intense Laser Pulses: Effective Potential Analysis of CO. *Front. Phys.* 9, 677671. doi:10.3389/fphy.2021.677671

Pertot, Y., Schmidt, C., Matthews, M., Chauvet, A., Huppert, M., Svoboda, V., et al. (2017). Time-Resolved X-ray Absorption Spectroscopy with a Water Window High-Harmonic Source. *Science* 264, 355. doi:10.1126/science.aah6114

Pfeifer, T., Walter, D., Winterfeldt, C., Spielmann, C., and Gerber, G. (2005). Controlling the Spectral Shape of Coherent Soft X-Rays. *Appl. Phys. B* 80, 277–280. doi:10.1007/s00340-005-1754-0

Ray, D., He, F., De, S., Cao, W., Mashiko, H., Ranitovic, P., et al. (2009). Ion-Energy Dependence of Asymmetric Dissociation of D_2 by a Two-Color Laser Field. *Phys. Rev. Lett.* 103, 223201. doi:10.1103/physrevlett.103.223201

Sato, Y., Kono, H., Koseki, S., and Fujimura, Y. (2003). Description of Molecular Dynamics in Intense Laser Fields by the Time-Dependent Adiabatic State Approach: Application to Simultaneous Two-Bond Dissociation of CO_2 and its Control. *J. Am. Chem. Soc.* 125, 8019–8031. doi:10.1021/ja0344819

Sheehy, B., Walker, B., and DiMauro, L. F. (1995). Phase Control in the Two-Color Photodissociation of HD^+. *Phys. Rev. Lett.* 74, 4799. doi:10.1103/physrevlett.74.4799

Song, Q., Gong, X., Ji, Q., Lin, K., Pan, H., Ding, J., et al. (2015). Directional Deprotonation Ionization of Acetylene in Asymmetric Two-Color Laser Fields. *J. Phys. B: At. Mol. Opt. Phys.* 48, 094007. doi:10.1088/0953-4075/48/9/094007

Takahashi, E. J., Lan, P., Mücke, O. D., Nabekawa, Y., and Midorikawa, K. (2010). Infrared Two-Color Multicycle Laser Field Synthesis for Generating an Intense Attosecond Pulse. *Phys. Rev. Lett.* 104, 233901. doi:10.1103/physrevlett.104.233901

Tang, X., Zhou, X., Wu, M., Gao, Z., Liu, S., Liu, F., et al. (2013). Dissociation Limit and Dissociation Dynamic of CF_4^+ : Application of Threshold Photoelectron-Photoion Coincidence Velocity Imaging. *J. Chem. Phys.* 138, 094306. doi:10.1063/1.4792368

Tolstikhin, O. I., Morishita, T., and Madsen, L. B. (2011). Theory of Tunneling Ionization of Molecules: Weak-Field Asymptotics Including Dipole Effects. *Phys. Rev. A* 84, 053423. doi:10.1103/physreva.84.053423

Walt, S. G., Ram, N. B., Conta, A. v., Tolstikhin, O. I., Madsen, L. B., Jensen, F., et al. (2015). Role of Multi-Electron Effects in the Asymmetry of Strong-Field Ionization and Fragmentation of Polar Molecules: The Methyl Halide Series. *J. Phys. Chem. A* 119, 11772–11782. doi:10.1021/acs.jpca.5b07331

Wanie, V., Ibrahim, H., Beaulieu, S., Thiré, N., Schmidt, B. E., Deng, Y., et al. (2015). Coherent Control of D_2/H_2 Dissociative Ionization by a Mid-Infrared Two-Color Laser Field. *J. Phys. B: At. Mol. Opt. Phys.* 49, 025601. doi:10.1088/0953-4075/49/2/025601

Winterfeldt, C., Spielmann, C., and Gerber, G. (2008). Colloquium: Optimal Control of High-Harmonic Generation. *Rev. Mod. Phys.* 80, 117–140. doi:10.1103/revmodphys.80.117

Wollenhaupt, M., and Baumert, T. (2011). Ultrafast Laser Control of Electron Dynamics in Atoms, Molecules and Solids. *Faraday Discuss.* 153, 9–26. doi:10.1039/c1fd00109d

Wu, J., Magrakvelidze, M., Schmidt, L., Kunitski, M., Pfeifer, T., Schöffler, M., et al. (2013). Understanding the Role of Phase in Chemical Bond Breaking with Coincidence Angular Streaking. *Nat. Commun.* 4, 2177. doi:10.1038/ncomms3177

Zare, R. N. (1988). *Angular Momentum*. New York: Wiley.

Conflict of Interest: The authors declare that the research was conducted in the absence of any commercial or financial relationships that could be construed as a potential conflict of interest.

Publisher's Note: All claims expressed in this article are solely those of the authors and do not necessarily represent those of their affiliated organizations or those of the publisher, the editors, and the reviewers. Any product that may be evaluated in this article, or claim that may be made by its manufacturer, is not guaranteed or endorsed by the publisher.